An Eulerian Method for Computing the Coherent Ergodic Partition of Continuous Dynamical Systems

Guoqiao You* Shingyu Leung†

June 20, 2013

Abstract

We develop an efficient Eulerian numerical approach to extract invariant sets in a continuous dynamical system in the extended phase space (the $\mathbf{x}-t$ space). We extend the idea of ergodic partition and propose a concept called *coherent ergodic partition* for visualizing ergodic components in a continuous flow. Numerically, we first apply the level set method [32] and extend the backward phase flow method [24] to determine the long time flow map. To compute all required long time averages of observables along particle trajectories, we propose an Eulerian approach by simply incorporating flow maps to iteratively interpolate those short time averages. Numerical experiments will demonstrate the effectiveness of the approach. As an application of the method, we apply the approach to the field of geometrical optics for high frequency wave propagation and propose to use the result from the coherent ergodic partition as a criteria for adaptivity in typical Lagrangian ray tracing methods.

1 Introduction

Ergodicity is an important concept in understanding dynamical systems [1, 9]. Roughly speaking, the term ergodic in mathematics is used to describe a dynamical system in which the time-average of all system states (in the phase space) has similar behavior to their space-average. In physics and statistical mechanics, it usually links to the *ergodic hypothesis* of thermodynamics which relates the time spent by a particle traveling in a certain region with the volume of that particular region [41, 2].

Although ergodic theory has been developed since Boltzmann in the 19th century [20], it has only come to the serious attention of the computational community recently. Following [29, 30], [25, 26] have developed a numerical approach to visualize the ergodic partition of **discrete** dynamical systems based on the ergodic partition theory. The algorithm first computes the time averages of various observables defined in the phase space, and then uses these averages to divide the phase space into a family of non-decomposable invariant sets in each of which all points are accessible from any initial takeoff location in the set. Roughly speaking, any particle in such an invariant set can arrive everywhere in the set at later times. To work on a **continuous** dynamical system, on the other hand, [39] has recently extended the theory of ergodic partition from [30] to analyze dynamics described by continuous-time nonlinear models such as fluid dynamics with time-dependent velocity profiles.

In this paper, we further extend that work by introducing a concept of *coherent ergodic partition*. We observe that for time-dependent flows, the partition will not necessarily be invariant sets in the phase space by simply computing the joint level sets of time averages of observables, and so the partition is in fact not ergodic. Having said that, all particles within the same partitioned component at a given time (all time averages are equal in the same component) should have very similar behaviors. This concept can still help us to better understand the structure of a dynamical system. For convenience, we will still call this partition an *ergodic partition*. We will further prove that although such ergodic partition depends on the initial referencing time, but the partition itself is coherent, i.e. the set follows the trajectories of the particles. This is the reason why we name such partition *coherent ergodic partition*. In [39], the authors have studied the so-called coherent swing instability (CSI) phenomenon and have shown that the corresponding ergodic partition is uniformly bounded. Here we extend the result and conclude that

*Department of Mathematics, the Hong Kong University of Science and Technology, Clear Water Bay, Hong Kong. Email: **gyou@ust.hk**

†Department of Mathematics, the Hong Kong University of Science and Technology, Clear Water Bay, Hong Kong. Email: **masyleung@ust.hk**

the *coherent ergodic partition* will form an invariant set in the extended phase space. Also, if the flow is periodic, the evolution of each ergodic component is periodic with the same period as the flow.

To numerically approximate the ergodic partition of a domain $\mathcal{M}$, one needs to compute the long time averages of a set of functions along particle trajectories. As a result, one has to compute the long time flow map of the corresponding dynamical system. All those methods we have mentioned above used a Lagrangian framework to compute the flow map, i.e. they all require to solve a system of ordinary differential equations (ODE's). In this work, however, we follow the Eulerian approach proposed in [21] which bases on the level set method [32] to compute the flow map defined on a fixed Cartesian mesh. The flow map satisfies a Liouville equation which can be solved by any well-established robust and high order accurate numerical methods, such as WENO5-TVDRK2 [28, 38, 12]. Based on this Eulerian formulation, we extend the approach to compute time averages of the observables along particle trajectories. For periodic flows, we further develop an efficient numerical approach to determine the required long-time integral based on the backward phase flow method in [24, 22]. Incorporating the level set method [32], the method can also be easily applied to compute the coherent ergodic partition on co-dimension one manifolds.

This paper is arranged as follows: In Section 2 we will summarize some definitions and a recently developed numerical method, which will be useful for the new developments we are proposing in this work. In Section 3, we will prove a coherent property of the coherent ergodic partition and we will also develop an efficient Eulerian algorithm to compute the ergodic partition at any initial referencing time. We will then carefully study the boundary conditions for the Eulerian approach in Section 4. We apply our proposed algorithm in Section 5 on several interesting and important dynamical systems, including the CSI, point vortex flow on sphere, double-gyre flow and also an application to geometrical optics for high frequency asymptotic wave propagation. We will also discuss the relationship between the chaotic property of the system and the distribution of the ergodic partition in the section.

2 Background

In this section, we will summarize several useful definitions and a recently developed numerical method, which will be useful for the new developments we are proposing in this work.

2.1 Ergodic partitions of phase space under a measure-preserving flow

In this subsection, we re-state some definitions and main results concerning ergodic partition of phase space. Let $\mathcal{M}$ be a compact metric space, $\mathcal{B}_\mathcal{M}$ be the Borel $\sigma-$ algebra of $\mathcal{M}$, and μ be an associated probability measure. Then the tuple $(\mathcal{M},\mathcal{B}_\mathcal{M},\mu)$ compose a probability space.

Definition 2.1 (Measure-preserving flow [39]). *A measure-preserving flow of the probability space is a group of measure-preserving diffeomorphisms ϕ_t for all $t\in\mathbb{R}$ such that each ϕ_t is measure-preserving in the sense $\mu(\phi_{-t}(B))=\mu(B)$ for all $B\in\mathcal{B}_\mathcal{M}$ and the following properties are satisfied: $\phi_0:\mathcal{M}\to\mathcal{M}$ the identity and $\phi_{t+s}=\phi_t\circ\phi_s$.*

Definition 2.2 (Partition and measure partition [30]). *A family ζ of disjoint sets whose union is identically $\mathcal{M}$ is called a partition of $\mathcal{M}$. Let A_α be an element of ζ where α is an element of some indexing set A. The partition ζ is called measurable if there exists a countable family Δ of measurable sets B_i such that (i) every B_i is a union of elements of ζ, and (ii) for every pair A_α, A_β of elements of ζ, there exists $B\in\Delta$ such that $A_\alpha\subset B$ and $A_\beta\subset B^c$.*

Definition 2.3 (Time average of a function f [39]). *Let f be a function defined on a compact metric space $\mathcal{M}$ and $\phi_t(x)$ be the underlying flow of a continuous dynamical system defined also on $\mathcal{M}$. If*

$$f^*(x)=\lim_{T\to\infty}\frac{1}{T}\int_0^T(f\circ\phi_t)(x)dt \tag{2.1}$$

exists a.e. on $\mathcal{M}$, then the function $f^*(x)$ is called the time average of f along the trajectories of the flow $\phi_t(x)$.

Lemma 2.4 (Existence of time average [39]). *For every $f\in C(\mathcal{M})$ and an arbitrary measure-preserving flow $\phi_t(x)$, f^* exists almost everywhere in $\mathcal{M}$. We denote Σ the set of all $x_0\in\mathcal{M}$ such that $f^*(x_0)$ exists, then the complimentary set Σ^c is surely of measure zero.*

Theorem 2.5 ([39]). *Let f be a continuous function on $\mathcal{M}$, then the family of sets $\{A_\alpha\}_{\alpha\in\mathbb{R}}$, where $A_\alpha := (f^*)^{-1}(\alpha)$, is a measurable partition of Σ and we denote it by ζ_f.*

Since different function f will lead to a different measurable partition of $\mathcal{M}$, we need the following definition of product operation.

Definition 2.6 (Product of partitions [30]). *Let ζ_1 and ζ_2 be two measurable partitions of $\mathcal{M}$, A_1 and A_2 be elements of ζ_1 and ζ_2, respectively, and also let ζ be the family of all sets of the form $A=A_1\cap A_2$. The partition ζ is also measurable and is called a product of partitions A_1 and A_2, denoted by $\zeta=\zeta_1\vee\zeta_2$.*

We further denote a finite (or countable) product by $\zeta=\bigvee_{i=1}^n\zeta_i$ for finite n or ∞. In [30], the authors have explained several lemmas and theorems about the theory of ergodic partition. These theories have then been extended to measure-preserving flows in [39]. Before defining the so-called ergodic given in [39], we do some notation convention: $L^1(\mathcal{M})$ denotes the space of all real-valued, $\mu-$ integrable functions on $\mathcal{M}$; $C(\mathcal{M})$ denotes the set of all real-valued, continuous functions on $\mathcal{M}$ and S denotes a dense countable subset of $C(\mathcal{M})$.

Definition 2.7 (Ergodic partitions [39]). *For a measurable partition ζ of $\mathcal{M}$, let A_α be an element of ζ where α is an element of some indexing set A as a measure space $(A,\mathcal{B}_A,P)$. The partition ζ is called ergodic under ϕ if*

1. *for almost every(with respect to μ) element A_α, it is invariant for ϕ and there exists an invariant probability measure μ_{A_α} on it such that for every $f\in L^1(\mathcal{M})$,*

$$\lim_{T\to\infty}\frac{1}{T}\int_0^T(f\circ\phi_t)(x)dt=\int_{A_\alpha}f d\mu_{A_\alpha},$$

   for almost everywhere with respect to μ_{A_α} on A_α, and

2. *for every $f\in L^1(\mathcal{M})$,*

$$\int_{\mathcal{M}}f\,d\mu=\int_A\left[\int_{A_\alpha}f\,d\mu_{A_\alpha}\right]dP(\alpha).$$

Roughly speaking, ergodic partition of the phase space $\mathcal{M}$ into invariant sets on which ϕ_t is ergodic. At this time, one question is naturally put forward: Does the ergodic partition exist for an arbitrary $\mathcal{M}$ and an arbitrary measure-preserving flow ϕ_t?

Theorem 2.8 (Existence of ergodic partition [39]). *Let ζ_e be the product of measurable partitions of Σ induced by every $f\in S$, i.e.*

$$\zeta_e=\bigvee_{f\in S}\zeta_f,$$

then the partition ζ_e together with Σ^c is ergodic under ϕ.

2.2 The backward phase flow method to compute the long time flow map

The original idea in the phase flow method [4] is based on the Lagrangian ODE ray tracing which might be problematic for flows in a bounded domain. In a recent paper [24], we have proposed a backward phase flow method for Eulerian flow map construction which is based on an Eulerian PDE formulation. This formulation provides a more natural way to handle the boundary condition. Solving the level set function Ψ **forward** in time, we obtain the *backward* flow map. In [24], we have developed an Eulerian method for the *backward* flow map construction by applying the phase flow method *backward* in time. Mathematically, we obtain the backward flow map from $t=T$ to $T-\Delta t$, $\Phi_{-\Delta t}:(x_i,p_j;T)\to(x(T-\Delta t),p(T-\Delta t);T-\Delta t)$ for some $\Delta t>0$ by solving the Liouville equation for Ψ forward in time from $t=T-\Delta t$ to $t=T$. Thus, if the flow is autonomous, the value of the phase flow map (the take off location of a bicharacteristic) at $t=T-2\Delta t$ with a terminate condition $(x,p)=(x_i,p_j)$ at $t=T$ can be computed by

$$\begin{aligned}&\Phi_{-2\Delta t}(x_i,p_j;T)=\Phi_{-\Delta t}(\Phi_{-\Delta t}(x_i,p_j;T))\\&=\Phi_{-\Delta t}\circ\Phi_{-\Delta t}(x_i,p_j;T)=\Phi^2_{-\Delta t}(x_i,p_j;T).\end{aligned}$$

Since that particular application [24] requires to recompute other physical quantities along with the backward flow map, we have not studied in details the map size doubling technique to speedup the long

time flow map computations. Therefore, we have implemented only the simple version of the backward flow map method which requires $\Phi_{-k\Delta t}(x_i,p_j;T)=\Phi^k_{-\Delta t}(x_i,p_j;T)$. Also, these two methods are proposed for autonomous systems in which the velocity model is independent of time. Therefore, Δt can be chosen arbitrarily.

In [22], we have recently extended the above approaches for autonomous and periodic flows. The idea for periodic flows is to develop a map doubling phase flow method for long time flow map computations. We first construct the solution $\Psi(\mathbf{x},T_m)$ by solving the Liouville equation

$$\frac{\partial\Psi(\mathbf{x},t)}{\partial t}+(\mathbf{u}\cdot\nabla)\Psi(\mathbf{x},t)=\mathbf{0} \tag{2.2}$$

forward in time from $t=0$ to $t=T_m$ for some time difference T_m. To determine $\Psi(\mathbf{x},2T_m)$, we use the phase flow property and obtain $\Psi(\mathbf{x},2T_m)=\Psi(\Psi(\mathbf{x},T_m),T_m)=\Psi\circ\Psi(\mathbf{x},T_m)$. In general, once we have obtained the solution $\Psi(\mathbf{x},2^{k-1}T_m)$, we can obtain $\Psi(\mathbf{x},2^kT_m)=\Psi(\Psi(\mathbf{x},2^{k-1}T_m),2^{k-1}T_m)$. Finally, if we take $T=2^mT_m$, the *backward* flow map $\Phi(\mathbf{x};2^mT_m,0)$ is given by $\Phi(\mathbf{x};2^mT_m,0)=\Psi(\mathbf{x},T)$.

The idea to compute the *forward* flow map is simple. We can solve the Liouville equation *backward* in time from $t=T$ to $t=T-T_m$. Then we iterate the map k-times to get the overall flow map *forward* in time from $t=0$ to $t=T=T_m\cdot 2^k$. Here, we summarize the backward phase flow method for *forward* flow map computation given in [22].

Algorithm 1: Computing the *forward* flow map $\Phi(\mathbf{x};0,2^mT_m)$ for a T_m-periodic flow with $T=2^mT_m$:

1. Construct $\Psi(\mathbf{x},(2^m-1)T_m)$ as in [21].
2. For $k=1,\cdots,m$, interpolate
$$\begin{aligned}\mathbf{y}&=\Psi(\mathbf{x},(2^m-2^{k-1})T_m)\\ \Psi(\mathbf{x},(2^m-2^k)T_m)&=\Psi(\mathbf{y},(2^m-2^{k-1})T_m).\end{aligned}$$
3. Set $\Phi(\mathbf{x};0,2^mT_m)=\Psi(\mathbf{x},0)$.

---

3 Coherent ergodic partition using the backward phase flow method

3.1 Coherent ergodic partition

In the original definition of ergodic partition in [30], the authors have only considered discrete dynamical systems. When generalizing the definitions to time-dependent continuous systems, we consider not only solutions at certain fixed initial referencing time but should also consider the solution at all other (initial) times.

Going back to the definitions given above, Definition 2.1 and Definition 2.2 can both be naturally extended to the periodic flows indeed. However, the extension of Definition 2.7 and Theorem 2.8 to a continuous dynamical system is straight-forward only if the flow is autonomous, i.e. time-independent. But if the flow is time-dependent (or even simply periodic), the extension does not always make sense. In fact, we will see in our examples, the partition corresponding to the product $\zeta_e=\bigvee_{f\in S}\zeta_f$ generally depends on the choice of the initial referencing time, which implies that the resulting components due to the partition are not really invariant. In other words, particles initially at one of these regions might leave the sub-domain at a later time, and particles initially located outside might enter these regions too. As a result, it is very difficult to know the partition at an arbitrary initial time. Nevertheless, we have the following lemma for both autonomous or time-dependent flows.

Lemma 3.1. *Let $\{\zeta^\tau|\tau\in\mathbb{R}\}$ be the partition of a **continuous dynamical system** at the initial referencing time $t=\tau$, i.e.*

$$\zeta^\tau=\bigvee_{f\in S}\zeta^\tau_f,$$

where ζ^τ_f denotes the measurable partition induced by $f\in S$ at initial time $t=\tau$. Then, components in $\{\zeta^{\tau_1}|\tau_1\in\mathbb{R}\}$ and $\{\zeta^{\tau_2}|\tau_2\in\mathbb{R}\}$ have one-to-one correspondence for arbitrary τ_1, $\tau_2\in\mathbb{R}$.

Proof. For arbitrary $x_0 \in \mathcal{M}$, let

$$f_\tau^*(x_0) \triangleq \lim_{T\to\infty} \frac{1}{T-\tau} \int_\tau^T (f \circ \phi_\tau^t)(x_0) dt, \tag{3.3}$$

then $f_{\tau_1}^*(x_0) = f_{\tau_2}^*(\phi_{\tau_1}^{\tau_2}(x_0))$ due to the boundedness property of each $f \in C(\mathcal{M})$. Let $A \in \zeta^{\tau_1}$ and $B \in \zeta^{\tau_2}$ be the components containing x_0 and $\phi_{\tau_1}^{\tau_2}(x_0)$ respectively, then A and B have the one-to-one correspondence in this sense: $x_1 \in A$ if and only if $\phi_{\tau_1}^{\tau_2}(x_1) \in B$. □

This lemma implies that each component of the partition evolves with the flow system. For periodic dynamical systems, we further have the following property.

Theorem 3.2. *Define $\{\zeta^\tau | \tau \in \mathbb{R}\}$ as in Lemma 3.1. We have $\zeta^\tau = \zeta^{\tau+T_m}$ for a periodic dynamical system with period T_m and arbitrary $\tau \in \mathbb{R}$.*

Proof. For arbitrary $x_0 \in \mathcal{M}$, from equation (3.3), we have

$$f_\tau^*(x_0) = \lim_{T\to\infty} \frac{1}{T-\tau} \int_\tau^T (f \circ \phi_\tau^t)(x_0) dt$$

and

$$f_{\tau+T_m}^*(x_0) = \lim_{T\to\infty} \frac{1}{T-(\tau+T_m)} \int_{\tau+T_m}^T (f \circ \phi_{\tau+T_m}^t)(x_0) dt.$$

Let $t' = t + T_m$, then

$$f_\tau^*(x_0) = \lim_{T\to\infty} \frac{1}{T-\tau} \int_{\tau+T_m}^{T+T_m} (f \circ \phi_\tau^{t'-T_m})(x_0) dt'.$$

Since the system is T_m-periodic, we have $\phi_\tau^{t'-T_m}(x_0) = \phi_{\tau+T_m}^{t'}(x_0)$, then

$$\begin{aligned} f_\tau^*(x_0) &= \lim_{T\to\infty} \frac{1}{T-\tau} \int_{\tau+T_m}^{T+T_m} (f \circ \phi_{\tau+T_m}^{t'})(x_0) dt', \\ &= \lim_{T\to\infty} \frac{1}{T-\tau} \int_{\tau+T_m}^{T} (f \circ \phi_{\tau+T_m}^{t})(x_0) dt, \\ &= \lim_{T\to\infty} \frac{1}{T-(\tau+T_m)} \int_{\tau+T_m}^{T} (f \circ \phi_{\tau+T_m}^{t})(x_0) dt, \\ &= f_{\tau+T_m}^*(x_0) \end{aligned}$$

which implies that $\zeta^\tau = \zeta^{\tau+T_m}$. □

With Lemma 3.1 and Theorem 3.2, we can easily partition the extended phase space of a periodic dynamical system with the partition at an arbitrary initial reference time $t = \tau$. In particular, we need to partition only at one time level at $t = t_0$, then we push forward the boundary of each connected component along their pathlines up to $t = t_0 + T_m$. Since the partition itself is T_m-periodic due to Theorem 3.2, we extend the partition periodically to obtain the partition for any time. Furthermore, in the *extended* phase space ($x-t$ space), boundary of each segmented component will form a tube-liked surface. In other words, a particle initially located outside this tube will always stay outside the tube, while a particle initially located within this tube will never leave it. That is why we say the partition for different initial times are invariant in the extended phase space. For convenience, we call this partition in the extended phase space the *coherent ergodic partition* and each component *ergodic component*, even though it may differs a bit from the original definition of the term *ergodic*. For the partition at a certain fixed time in the phase space, we still call the partition the *ergodic partition* as before.

However, there is no guarantee that each ergodic component is connected at a given time. As we will see later in our examples, an ergodic component could be a collection of discrete points, or a union of several connected components, or even a combination of them. We observe that the topology of the coherent ergodic partition depends on how *chaotic* the system is. For instance, an autonomous system could be much *less chaotic* than a non-autonomous one. We will give an example in which the system is so *chaotic* that we cannot observe any obvious connected component.

However, because the flow map $\phi_{\tau_1}^{\tau_2}$ for arbitrary $\tau_1, \tau_2 \in \mathbb{R}$ is continuous and is area-preserving, the connectivity and the measure of each set should be preserved.

3.2 Relation with the finite time Lyapunov exponent (FTLE) field

Since our coherent ergodic partition tries to extract invariant sets in a dynamical system, it is natural to expect that the method relates to other coherent structure identifying methods. For instance, we have observed that our coherent ergodic partition closely relates to the finite time Lyapunov exponent (FTLE) [18, 15, 16, 37, 17, 21]. FTLE is one of many possible Lagrangian quantities which can be used to detect the so-called Lagrangian coherent structure (LCS). It measures the rate of separation between adjacent particles over a finite time interval with an infinitesimal perturbation in the initial location. In practice, the first step to compute the FTLE is to move particles in the flow for a period of time and obtain the flow map which takes the initial particle location to it's arrival location. Then the FTLE is computed based on the Jacobian of the flow map.

One hint for the relationship is in the Lagrangian property of these concepts. For $T\to\infty$, the FTLE reduces to the traditional Lyapunov exponent which is hyperbolic according to the Oseledec's multiplicative ergodic theorem, see also [37]. Such hyperbolic property exists also in our coherent ergodic partition. As we have proved above, the ergodic partition of different initial referencing time is hyperbolic, i.e. it's boundary follows particle trajectories, and therefore coherent.

Numerically, as will also be demonstrated in Section 5, we have found that the shape of our coherent ergodic components at different $t=t_0$ coincides very well with the FTLE field $\sigma_{t_0}^T$ for large enough T. In particular, in a region with extremely large FTLE value, the particle trajectory will be very sensitive to initial perturbation. This implies that a small change in the initial location of the particle will lead to a very different trajectory. Therefore, the integral F will be very different and so F will change significantly in that particular region. On the other hand, in a region where FTLE is small, particles will tend to travel as a patch and so the integral F will have similar value.

This phenomena is definitely not too surprising because both concepts try to identify coherent structures in the flow. For example, the ergodic quotient in [3] has pointed out explicitly that the computed quantity closely relates to the coherent structure in flows. The transfer operator approach in [11] has also detected almost-invariant sets and invariant manifolds which have been shown to connect to the coherent structures. However, these two works consider only the relationship at **a fixed given time**. In this work, however, we are considering the similarity of these solutions in the whole extended phase space and we emphasize on the hyperbolicity of the structure.

3.3 A numerical approach based on the backward phase flow method

The coherent ergodic partition divides the extended phase space into a family of invariant sets. To obtain the whole coherent ergodic partition for different time levels, we need to know the partition at one initial time first. Given any continuous periodic dynamic system, we here present a numerical method to approximate the ergodic partition at one initial time (e.g. $t_0=0$) by computing the time averages of several functions using an Eulerian method.

Pick several functions $\{f_k|k=1,2,...,m,m\in\mathbb{Z}\}$ properly from $L^1(A)$ and compute the integration of each f_k for each particle, i.e.

$$F_k(\mathbf{x},t)=\int_0^t (f_k\circ\phi_t^\tau)(\mathbf{x})d\tau$$

where $F_k(\mathbf{x},t)$ denotes the integration of the function f_k from 0 to t along the particle trajectory which passes through $\mathbf{x}$ at time t. Then we have

$$\frac{dF_k}{dt}=f_k(\mathbf{x})$$

or

$$(F_k)_t+\mathbf{u}\cdot\nabla F_k=f_k(\mathbf{x}). \tag{3.4}$$

To solve the above equation for a very long time T for a periodic $\mathbf{u}$, we extend the backward phase flow method proposed in [22]. The idea is as follows. We first solve equation (3.4) with the initial condition $F(\mathbf{x},0)=0$ up to $t=T_m$, where T_m is the period of the periodic system, or simply an arbitrary constant for autonomous system. In implementation, this equation can be solved together with the flow map equation (2.2) in step 1 from Algorithm 1. At $t=T_m$, the quantity $F(\mathbf{x},T_m)$ denotes the value of the definite integral $\int_0^{T_m} f(\mathbf{y}(\tau))d\tau$ with $\mathbf{y}(T_m)=\mathbf{x}$ satisfying the ordinary differential equation $\mathbf{y}'(t)=\mathbf{u}(t)$. And therefore, we have

$$F(\mathbf{x},T_m)=\int_0^{T_m} f(\phi_{T_m}^\tau(\mathbf{x}))d\tau. \tag{3.5}$$

Now, to obtain $F(\mathbf{x},2T_m)$, we propose here an iterative approach based on the periodic structure of the flow. In particular, we have

$$\begin{aligned}
F(\mathbf{x},2T_m) &= \int_0^{2T_m} f(\phi^{\tau}_{2T_m}(\mathbf{x}))d\tau \\
&= \int_{T_m}^{2T_m} f(\phi^{\tau}_{2T_m}(\mathbf{x}))d\tau + \int_0^{T_m} f(\phi^{\tau}_{2T_m}(\mathbf{x}))d\tau \\
&= \int_0^{T_m} f(\phi^{\tau}_{T_m}(\mathbf{x}))d\tau + \int_0^{T_m} f(\phi^{\tau}_{T_m}(\phi^{T_m}_{2T_m}(\mathbf{x})))d\tau \\
&= F(\mathbf{x},T_m) + \int_0^{T_m} f(\phi^{\tau}_{T_m}(\phi^{0}_{T_m}(\mathbf{x})))d\tau \\
&= F(\mathbf{x},T_m) + F(\phi^{0}_{T_m}(\mathbf{x}),T_m).
\end{aligned}$$

The first term in the expression is the solution we obtained immediately from solving the partial differential equation (3.4). The second term $F(\phi^0_{T_m}(\mathbf{x}),T_m)$ can be easily determined by using any well developed monotone interpolation scheme.

For later time $t=T_m2^n$, we have

$$F(\mathbf{x},T_m2^n) = F(\mathbf{x},T_m2^{n-1}) + F(\phi^0_{T_m2^{n-1}}(\mathbf{x}),T_m2^{n-1}).$$

The computational algorithm is as follows:

Algorithm 2 (An Eulerian Method for computing functions F_k for T_m-periodic flows):

1. Discretize the computational domain

$$\begin{aligned}
&x_i = x_{\min} + (i-1)\Delta x, \quad \Delta x = \frac{x_{\max}-x_{\min}}{I-1}, \quad i=1,2,...,I, \\
&y_j = y_{\min} + (j-1)\Delta y, \quad \Delta y = \frac{y_{\max}-y_{\min}}{J-1}, \quad j=1,2,...,J, \\
&t_k = k\Delta t, \quad \Delta t = \frac{T}{K}, \quad k=0,1,...,K.
\end{aligned}$$

2. Initialize the level set functions

$$\begin{aligned}
\Psi^1(x_i,y_j,0) &= x_i, \\
\Psi^2(x_i,y_j,0) &= y_j, \\
F_k(x_i,y_j,0) &= 0, \quad k=1,2,...,m.
\end{aligned}$$

3. Solve equations (2.2) and (3.4) up to $t=T_m$ to get $\phi^0_{T_m}(\mathbf{x})$ and $F_k(\mathbf{x},T_m)$.

4. Obtain $F_k(\phi^0_{T_m}(\mathbf{x}),T_m)$ from $F_k\ (\mathbf{x},T_m)$ by interpolation. For T_m-periodic flows,

$$F_k(\mathbf{x},2T_m) = F_k(\mathbf{x},T_m) + F_k(\phi^0_{T_m}(\mathbf{x}),T_m).$$

5. Repeat step 4 until $t=t_{ex}=T_m2^n$ to get $F_k(\mathbf{x},t_{ex})$.

Remark 1. Theorem 3.2 guarantees that $\frac{1}{t_{ex}}F_k(\mathbf{x},t_{ex})$ converges to $(f_k)^*_0$ as $n\to\infty$. In our numerical experiments, we find that $\frac{1}{t_{ex}}F_k(\mathbf{x},t_{ex})$ approximates $(f_k)^*_0$ extremely well even when $n=4$ or 5.

Remark 2. Once we have obtained $F_k(\mathbf{x},t_{ex})$, various clustering algorithms can be applied to perform the segmentation, such as the EM algorithm based on the Gaussian mixture model [14, 5, 33], the total variation (TV) regularization approaches [36, 6, 8], or a combination of these statistical and PDE approaches [23, 27]. In this paper, we following the approach in [27].

4 Comments on the boundary condition for the Eulerian computations

Numerically, velocity field might be available only in certain bounded computational domain. We have proposed the following boundary condition for the Eulerian approach in [21] for $t>t_0$,

$$\Phi(\mathbf{x},t)|_{\mathbf{x}\in\partial\Omega}=\Phi(\mathbf{x},t_0)|_{\mathbf{x}\in\partial\Omega}=\mathbf{x}$$

if $\mathbf{n}\cdot\mathbf{u}<0$ where $\mathbf{n}$ is the outward normal of the boundary, and

$$\mathbf{n}\cdot\nabla\Phi^i(\mathbf{x},t)|_{\mathbf{x}\in\partial\Omega}=0$$

for $i=1,\cdots,d$ if $\mathbf{n}\cdot\mathbf{u}>0$. The first constraint imposes the inflow condition for which all incoming information will carry the location where the corresponding characteristics enter the computational domain. Consider an interior grid point (x_i,y_j,t_k) on a characteristic hitting the computational boundary at $t\in[t_0,t_k)$ when tracing backward in time. The corresponding value of $\Psi(x_i,y_j,t_k)$ will contain the precise location where the particle entered the domain.

On the boundary with $\mathbf{n}\cdot\mathbf{u}>0$, information is out-going from the interior and no boundary condition is required. For the ease of numerical implementations, we have simply imposed in [21] a non-reflective boundary condition so that no information on this portion of the boundary will interfere with function values at the interior.

In practice, because of the above boundary condition, the value Ψ at a grid point on the initial time level $t=t_0$ might represent either the take-off location of the particle or the location on the boundary $\partial\Omega$ where the particle entered the computational domain. This might be problematic in applications, such as the artificial FTLE ridge [21]. In this paper, we propose two numerical strategies to further take care of the influence due to the boundedness of the computational domain.

The first approach is to further incorporate a function $\mathcal{T}$ satisfying

$$\mathcal{T}_t+\mathbf{u}\cdot\nabla\mathcal{T}=0 \tag{4.6}$$

with the initial condition $\mathcal{T}(x,y,t_0)=t_0$ and the boundary condition

$$\mathcal{T}(\mathbf{x},t)|_{\mathbf{x}\in\partial\Omega}=t$$

for $\mathbf{n}\cdot\mathbf{u}<0$ and $t>t_0$. Following the argument as before, even though there is no need to impose any boundary condition for the part where $\mathbf{n}\cdot\mathbf{u}>0$, we still impose the same boundary condition for the ease of numerical implementations. Solution to (4.6) satisfies $D\mathcal{T}/Dt=0$ which implies that $\mathcal{T}$ is constant along characteristics. If a characteristic does not touch the boundary $\partial\Omega\times[t_0,\infty)$, $\mathcal{T}$ is given by the initial condition which is t_0. If a characteristic enters the domain on the boundary $\partial\Omega$ at the time $t=t^*$, then the value $\mathcal{T}$ will be t^*. Therefore, solution to (4.6) in fact can be used to distinguish whether Ψ represents the take-off location of the particle (if $\mathcal{T}=t_0$) or whether Ψ records the location on $\partial\Omega$ where the characteristic enters the domain (if $\mathcal{T}>t_0$). For instance, in [21] when we want to get rid of the artificial FTLE ridge, we could solve (4.6) together with the level set equations for the flow map. If $\mathcal{T}>t_0$ at the FTLE ridge, we will then ignore the solution.

The above approach in fact gives the exact time when the characteristic has entered the domain. This might not be necessary in practice if we just want to identify certain part of the domain which has been influenced by the boundary of the computational domain. A more direct approach relies on Ψ itself. We have noticed that Ψ at a time $t>t_0$ cannot represent a take-off location in the interior of Ω if $\Psi\in\partial\Omega$. This gives a very convenient tool to label a subdomain in Ω where there is no one-to-one correspondence between a point on $t=t_0$ and $(\mathbf{x},t)$ jointed by a characteristic staying inside Ω for all time between t_0 and t.

This is important in the current application when computing the quantity F since equation (3.5) holds only if $\phi^0_{T_m}$ makes sense. Numerically, because the computational domain is always bounded, one might not be able to determine a backward flow map $\phi^0_{T_m}$ joining any point on $t=T_m$ to the initial referencing time $t=0$. Therefore, (3.5) might not be correctly interpreted by solving equation (3.4) with the initial condition $F(\mathbf{x},0)=0$ and the boundary condition $F(\mathbf{x},0)|_{\mathbf{x}\in\partial\Omega}=0$. In particular, the solution actually denotes

$$F(\mathbf{x},T_m)=\int_{t^*}^{T_m} f(\phi^\tau_{T_m}(\mathbf{x}))d\tau$$

where t^* is the time when the characteristic has entered the domain. Because there is no information from the Eulerian flow map where the ray traveled before entering to the domain, we cannot use the computed $F(\mathbf{x},T_m)$ for ergodic partition. Therefore we will simply identify those regions by checking if $\Psi \in \partial\Omega$. If so, we will ignore the partition from those subdomains.

5 Numerical examples

5.1 Coherent swing instability (CSI)

In this example we follow [39] to characterize the coherent swing instability (CSI) phenomenon by considering the following planar dynamical system

$$\begin{aligned}\frac{d\delta}{dt} &= w,\\ \frac{dw}{dt} &= p_m - \frac{b}{N}\sum_{i=1}^{N}\sin\Big(\sum_{j\in J} e_{ij}c_j\cos(\Omega_j t)+\delta\Big),\end{aligned}$$

where $e_{ij}=\sqrt{\frac{2}{N}}\cos(\frac{2\pi ij}{N}+\frac{\pi}{4})$, $\Omega_j=2\sqrt{|b_{int}|}|\sin\frac{\pi j}{N}|$, $p_m=0.009$, $b=0.01$, $N=20$, $b_{int}=1$.For a complete description of the system and parameters, we refer interested readers to [39].

The above system is quasi-periodic. However, we here consider the situation when $J=1$ and $c_j=1$ under which the system is periodic with period $T_m=\frac{2\pi}{\Omega_1}$. Numerically, according to Algorithm 2, we solve all the level set equations up to T_m where we use only one single function $f=\sin(2\delta)$ following [39]. Then we interpolate our results 4 times (i.e. $n=4$ in Algorithm 2) to obtain corresponding $F(t_{ex},x)$ with $t_{ex}=\frac{32\pi}{\Omega_1}$ which approximates $t_{ex}f^*$ at the initial referencing time $t_0=0$. In summary, we obtain the flow map for a small period $T_m=\frac{2\pi}{\Omega_1}$ and then apply the backward phase flow method for long time propagation.

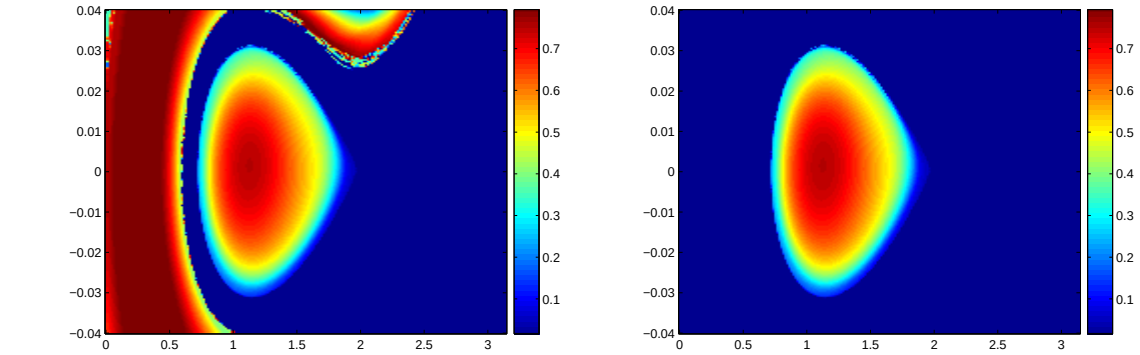

(a) (b)

Figure 1: (Section 5.1) Ergodic partition of the phase space at $t_0=0$ in the measure-preserving flow defined by this system. (a) Some regions are influenced by the boundary. (b) Solution after the boundary treatment in the Eulerian flow map construction.

It can be seen from Figure 1(a) that some regions are influenced by the Eulerian computation due to the presence of the boundary condition. The results from [39] are based on Lagrangian tracing where numerical integration of the planar system is performed with the 4-th order explicit symplectic integrator and thus they do not need boundary conditions. On the other hand, we use an Eulerian formulation where boundary conditions are necessary for solving the PDE's. As discussed in Section 4, numerical solution from certain subdomain is seriously influenced by the boundary condition in the Eulerian approach. We will therefore only trust the partition when $\phi(\mathbf{x},t)\notin\partial\Omega$. Figure 1(b) shows the result where those regions influenced by the boundary condition have been ticked out and it is consistent with those given in [39]. Like [39], the background (blue) color region implies that each trajectory from it diverges as time passes.

However, Figure 1(b) only shows the ergodic partition at one initial time $t_0=0$, we still need to put forward the solution along the particle trajectories up to $t=T_m$ in order to obtain the ergodic partition at all intermediate times, i.e. the coherent ergodic partition which is shown in Figure 2 (a). It seems that the ergodic partition keeps the same for all intermediate times. In other words, the subregions

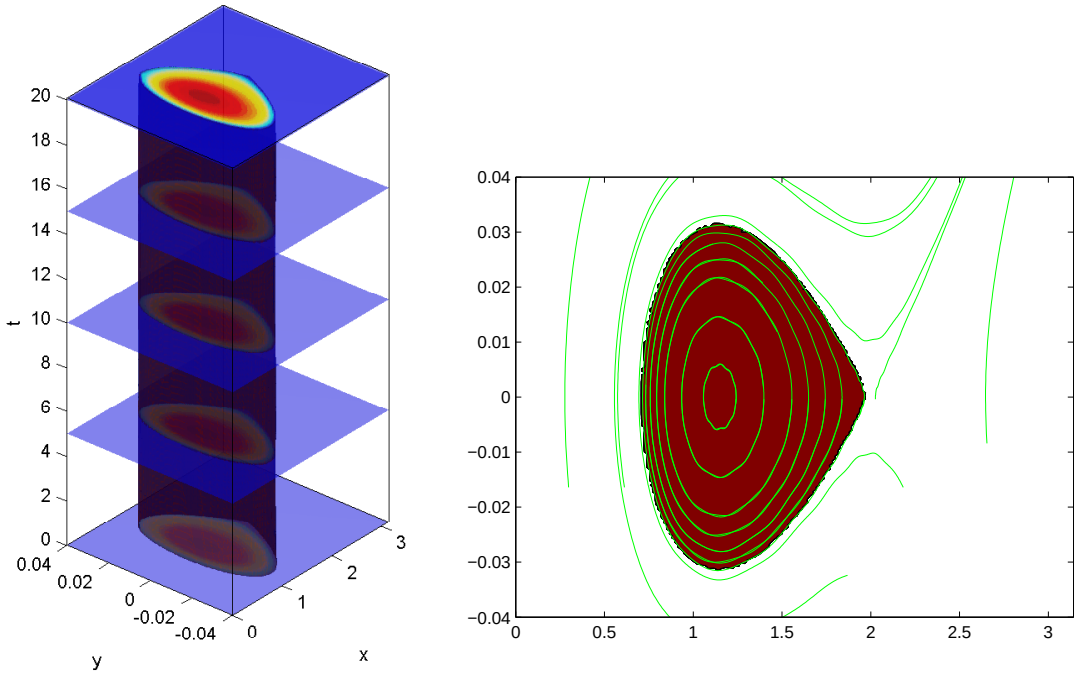

Figure 2: (Section 5.1) (a) The coherent ergodic partition within one period. (b) Several particle trajectories.

partitioned (the subregion where no CSI phenomenon happens) are invariant sets. In Figure 2 (b), we have plotted several particle trajectories within the red region where no CSI phenomenon has happened. These trajectories are almost closed curves which coincides with the observation that the red region seems like an invariant set.

5.2 Point vortex flow on a sphere

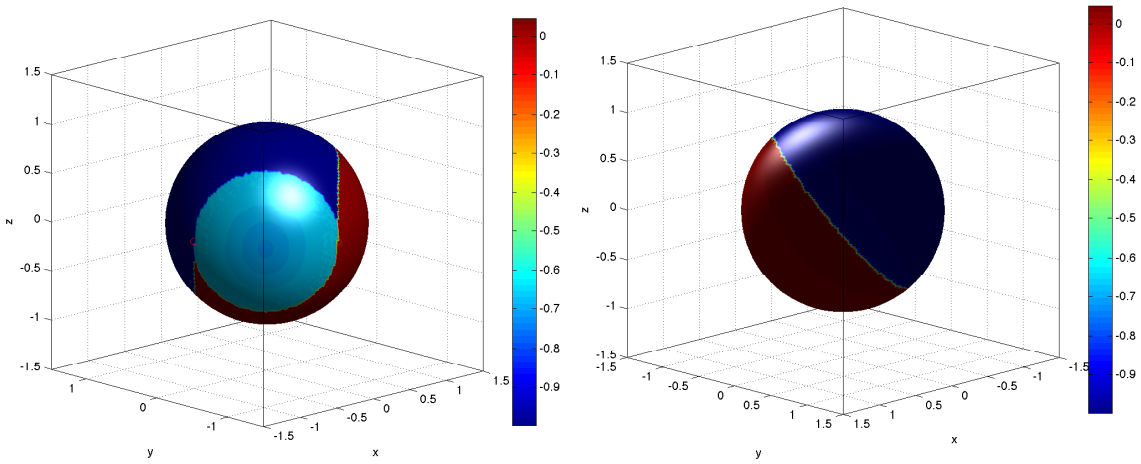

Figure 3: (Section 5.2) Ergodic partition on a sphere for the point vortex flow using $f(x,y,z)=x$, front and back.

It is also relatively straight-forward to compute the ergodic partition on a codimension one manifold in the proposed framework. Instead of triangulating the surface in a typical Lagrangian method, we following the level set approach as in [21] to implicitly represent the orientable and closed manifold by the zero level set of a level set function.

In this example, we consider an advection motion in a field of the two point vortices on a sphere of radius 1 centered at the origin [31]. The velocity of a particle on the manifold satisfies the motion

$$\mathbf{x}' = \frac{1}{2\pi}\sum_{i=1}^{2}\frac{\mathbf{x}_i \times \mathbf{x}}{2(1-\mathbf{x}_i\cdot\mathbf{x})}$$

with two point vortices placed at $\mathbf{x}_1 = (-1,0,0)$ and $\mathbf{x}_2 = (0,-1,0)$. We follow the same Eulerian idea proposed earlier [21] to represent the sphere in $\mathbb{R}^3$ implicitly using the level set function $\phi(x,y,z) = \sqrt{x^2+y^2+z^2}-1$. The first step is to extend the velocity field from the sphere to the whole computational domain, or at least a small computational tube near the sphere. We choose here the natural extension such that the velocity at a grid point is the same as that at it's L_2-projection onto the sphere. Then the flow map is computed on the uniform Cartesian mesh without explicitly triangulating the surface. To compute the integral of an observable along a particle, we can simply extend equation (3.4) naturally from the manifold to the whole computational domain. To have a numerically stable solution, at each timestep $t = t^k$, we also solve the same equation like the flow map extension, i.e. we solve the following equation for several time marching steps

$$\tilde{F}_\tau + \mathrm{sgn}(\phi)(\mathbf{n}\cdot\nabla)\tilde{F} = 0$$

for some artificial time τ up to τ^* and the initial condition $\tilde{F}(\mathbf{x},\tau=0) = F(\mathbf{x},t^k)$, and then replace the solution $F(\mathbf{x},t^k)$ by $\tilde{F}(\mathbf{x},\tau^*)$. This extension technique has been used very commonly in the level set community [32].

Figure 3 shows the ergodic partition on the surface computed using the proposed backward phase flow method at $t = 2048$ on an underlying uniform mesh of size $\Delta x = \Delta y = \Delta z = 3/128$. We first compute the flow map at $t = T_m = 2^{-4}$ and then iterate the map 15 times to obtain the final flow map at $t = T_m \cdot 2^{15}$. We have also plotted the location of the point vortices in small red circles. The sphere is clearly partitioned into 3 subregions with the point vortices located at the triple junctions of the partition.

5.3 Double-gyre flow

This example is taken from [37] to describe a periodically varying double-gyre. The flow is modeled by the following stream-function

$$\psi(x,y,t) = A\sin[\pi g(x,t)]\sin(\pi y), \tag{5.7}$$

where

$$\begin{aligned} g(x,t) &= a(t)x^2 + b(t)x, \\ a(t) &= \epsilon\sin(\omega t), \\ b(t) &= 1 - 2\epsilon\sin(\omega t). \end{aligned} \tag{5.8}$$

In this example, we follow [37] and use $A = 0.1$, $\omega = 2\pi/10$. We discretize the domain $[0,2]\times[0,1]$ using 513 grid points in the x-direction and 257 grid points in the y-direction. This gives $\Delta x = \Delta y = 1/256$. Using the backward phase flow method, we first solve the level set equations from $t = t_0 = 0$ to $t = T_m = 10$ and then iterate the flow maps 5 times to get $F(\mathbf{x},t_{ex})$ for $t_{ex} = T_m 2^5 = 320$. In Figure 4(a), we have shown the quantity $\frac{1}{320}F(\mathbf{x},320)$ using $f(\mathbf{x}) = \cos(2\pi y)$ with no perturbation, i.e. $\epsilon = 0.0$. The flow is autonomous and therefore the theories from [30, 39] can be directly applied. We have also plotted several particle trajectories in Figure 4(b), and these solutions match well with the solution in (a). We further remark that the ergodic partition in Figure 4(a) is invariant in the phase space because the underlying flow is autonomous.

To see the effect of the perturbation in the mixing, we use the same set of parameters as in [37, 21] by increasing ϵ to 0.1. We obtain $\frac{1}{320}F(\mathbf{x},320)$ with $f = \cos(2\pi y)$ and the solution is shown in Figure 5. The quantitative behavior of the solution is now changed significantly. For instance, the whole computational domain is now roughly partitioned into several regions including two circular regions centered near (0.5,0.5) and (1.5,0.5), two arrow regions slightly below and slightly above these two circular regions respectively, and also the background region which contains many isolated dots. Within each of these regions, the averaged value of F shows similar quantity. To better distinguish these regions, we use four independent test functions $f_1 = \cos(2\pi y)$, $f_2 = \cos(12\pi x)\cos(2\pi y)$, $f_3 = \sin(2\pi y)$, and $f_4 = \frac{x}{2}$, and segment these $\mathbb{R}^4$ data into several clusters with the geometrical constraint in $\mathbb{R}^2$ (Figure 6). For grid points within the same cluster, we color it using the same gray-level intensity, i.e. each group is colored

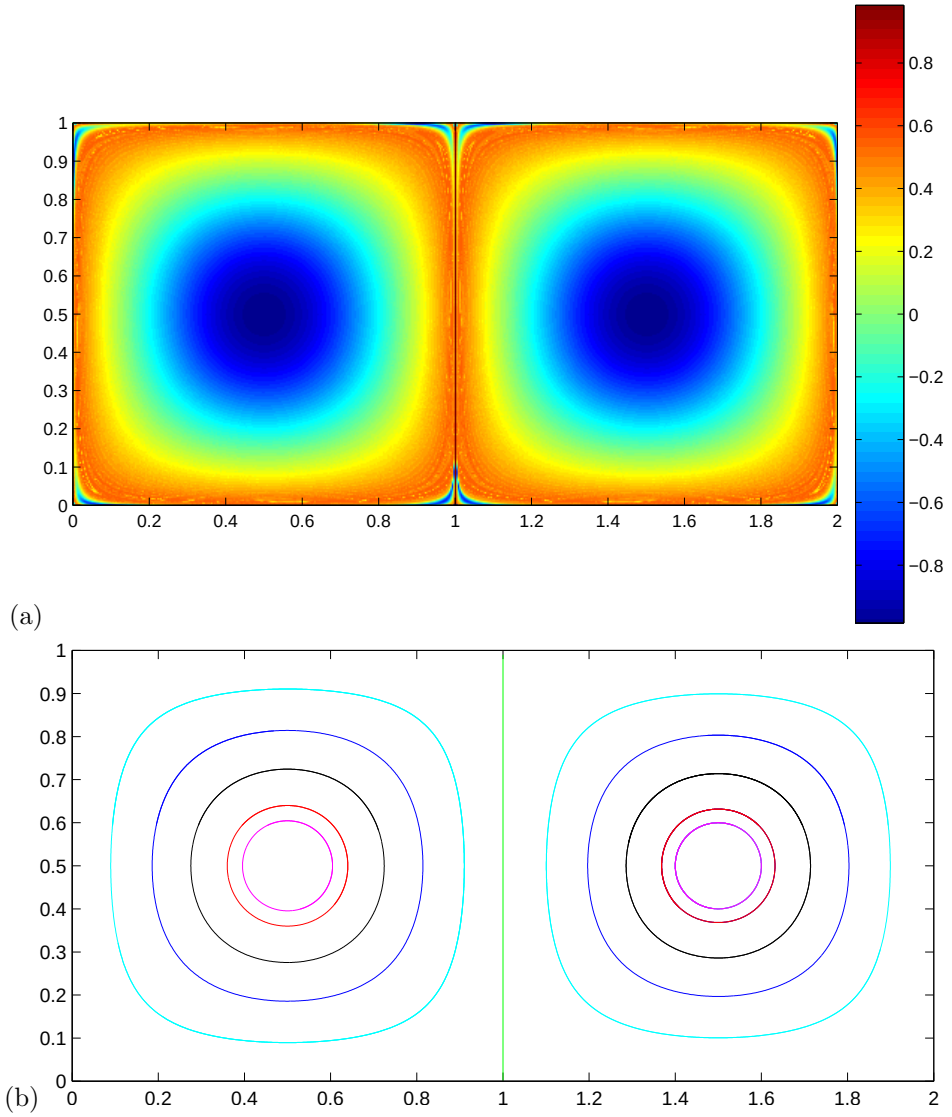

Figure 4: (Section 5.3 with $\epsilon=0.0$) (a) Contour plot of $\frac{1}{t_{ex}}F(\mathbf{x},t_{ex})$ with $f(\mathbf{x})=\cos(2\pi y)$. (b) Several particle trajectories following the time-independent flow.

in the same intensity. Our method can nicely classified the domain into various subregions according to $\mathbf{F}=(F_1,F_2,F_3,F_4)$ denoting the averaged value of the integrals with respect to the test functions f_1 to f_4, respectively.

However, since the dynamical system is time-dependent, as we said before, the result from the ergodic partition depends on the initial referencing time. In Figure 7(a), we show the evolution of the four connected components in Figure 6 from $t=0$ to $t=10$, i.e. the coherent ergodic partition of the flow. To better demonstrate the property of the coherent ergodic partition, we have plotted in Figure 7(b-d) several particle trajectories in the $\mathbf{x}-t$ domain(extended phase space) and showed that these trajectories will not penetrate any of these partition boundaries. For instance, in Figure 7(b), two particles initially locate inside the circular regions will remain inside the circular tube for all time between 0 and 10. Figure 7(c) and (d) show several other particle trajectories within the arrow-like region and the background region. All these rays will stay within the same class for all time. In other words, Figure 7(b-d) shows that the coherent ergodic partition of periodic dynamical systems for all different times form an invariant set in the extended phase space. Furthermore, from Figure 7(a) we can see that the slices of $t=0$ and $t=10$ are the same which indicates that the ergodic partitions at $t=0$ and $t=10$ are the same. This is consistent with our Theorem 3.2 by letting $\tau=0$ and $T_m=10$.

Even though the evolution of these boundaries are periodic and the trajectory itself in the $\mathbf{x}-t$ space cannot leave the partition regions, the trajectory of each individual particle itself is not necessarily periodic. To better demonstrate this, we have plotted in Figure 8 the location of those particles in Figure

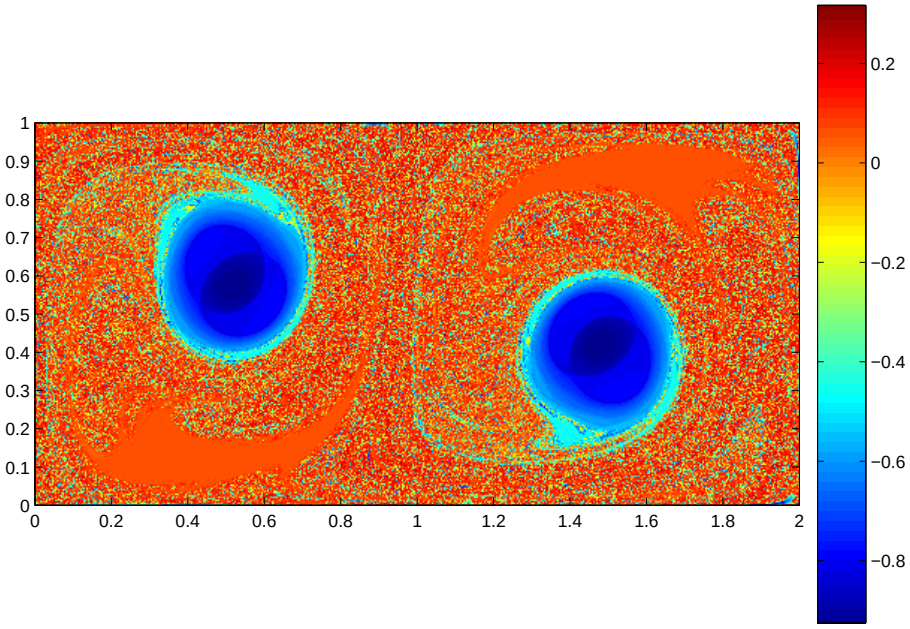

Figure 5: (Section 5.3 with $\epsilon=0.1$) $\frac{1}{t_{ex}}F(\mathbf{x},t_{ex})$ with $f(\mathbf{x})=\cos(2\pi y)$.

Figure 6: (Section 5.3 with $\epsilon=0.1$) Ergodic partition at $t=0$ with $\mathbf{F}=(F_1,F_2,F_3,F_4)$ using $t_{ex}=320$.

7 at constant multiples of the period $T_m=10$. If the motion of a particle is periodic with period T_m, we should see only one single location in the graph for each individual initial location. However, as we can see, particles tend to reach everywhere in each connected segment.

Figure 9 shows the result of ergodic partition of the double-gyre flow with $\epsilon=0.1$ at initial time $t_0=2.5$. According to Lemma 3.1, this partition at $t=2.5$ should be the evolution of the partition at $t=0$ after 2.5 temporal units and we have confirmed it by comparing it to the $t=2.5$ slice of Figure 7(a). Figure 10 is the evolution of the clusters in Figure 9 from $t=2.5$ to $t=12.5$. We can see that the coherent ergodic partition from $t=2.5$ to $t=12.5$ is exactly the coherent ergodic partition from $t=0$ to $t=10$ by cutting the part from $t=0$ to $t=2.5$ and put it on the remaining part from $t=2.5$ to $t=10$. This verifies that to know the coherent ergodic partition for all initial times, we only need to do the partition for one arbitrary initial time $t=t_0$ and then put forward the partition along the pathlines up to $t=t_0+T_m$.

Here, we also comment on the use of the ergodic partition as a tool for measuring the *level of chaos* in a dynamical system. In Figure 11 we have shown the quantity $\frac{1}{t_{ex}}F(\mathbf{x},t_{ex})$ using $f(\mathbf{x})=\cos(2\pi y)$ for different magnitudes of the perturbation from $\epsilon=0.003$ to a very large magnitude of disturbance $\epsilon=1.2$. For large value of ϵ, we hardly see any large connected component. This implies that for almost any initial location at $t=0$, a tiny perturbation in the location will lead to a very different trajectory in the $\mathbf{x}-t$ space. This gives us a hint that the coherent ergodic partition can be used as a tool to quantify how

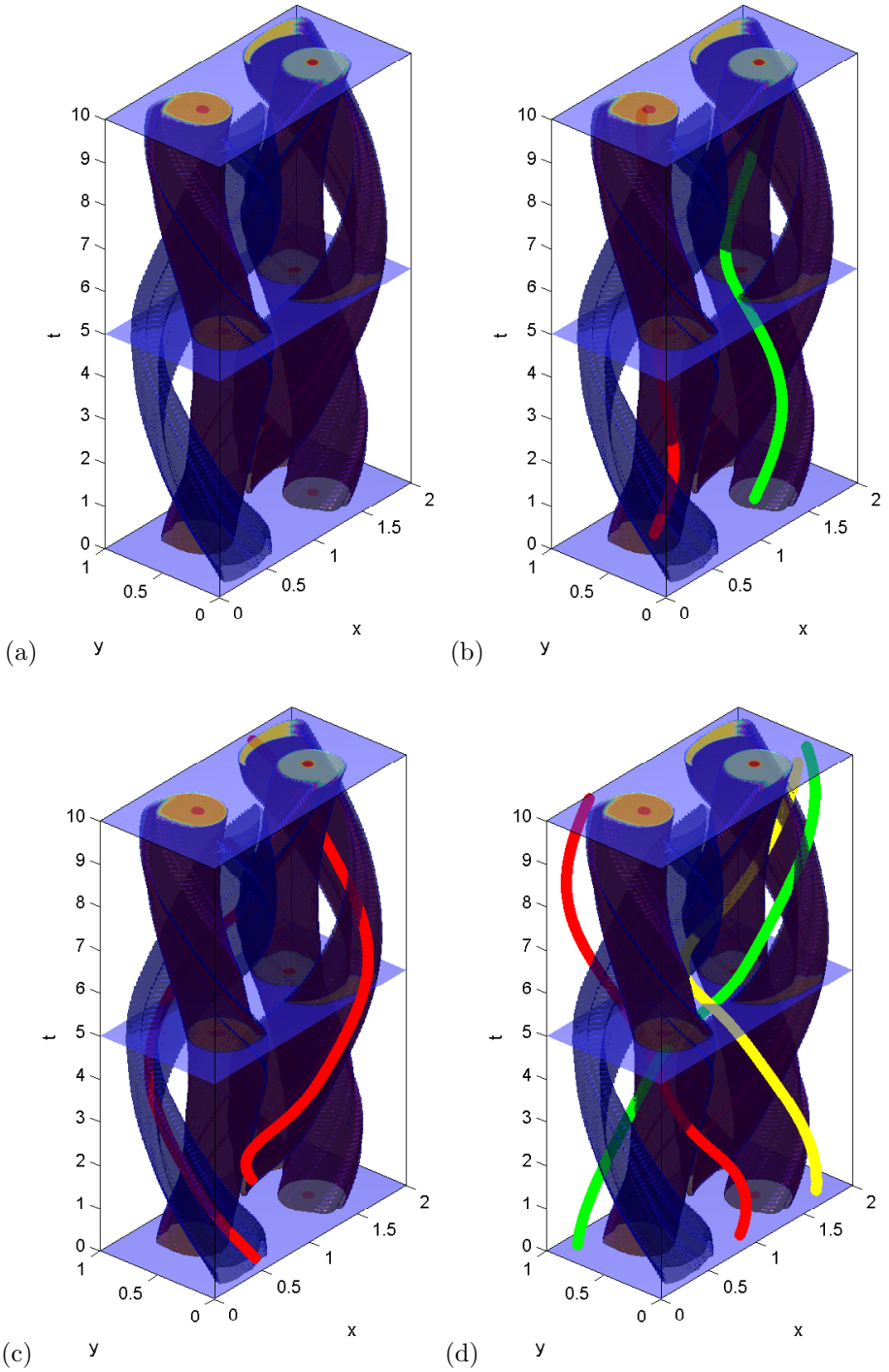

Figure 7: (Section 5.3 with $\epsilon = 0.1$) (a) The evolution of the clusters in Figure 6 from t=0 to t=10. (b) Two particles initially located at (1.3945,0.39453) and (0.59375,0.59766) will stay in the two circular tubes. (c) Two particles initially located at (1.3945,0.84375) and (0.59375,0.14453) will stay in the two arrow-like tubes. (d) Three particles initially located at (1.793,0.14453), (0.19531,0.89453) and (0.99609,0.14453) will stay outside four tubes.

chaotic a system is. The larger the region containing disconnected dots, the more *chaotic* the system is. If there is no obvious connected components, the system is *very chaotic*.

Finally, we shown in Figure 12 the forward FTLE on the level $t = 0$ with $T = 320$, i.e. $\sigma^{320}(\mathbf{x},0)$. One can compare it with Figure 5. For the region when FTLE is large (the background region), small perturbation in the initial condition will lead to a very different trajectory and so the corresponding

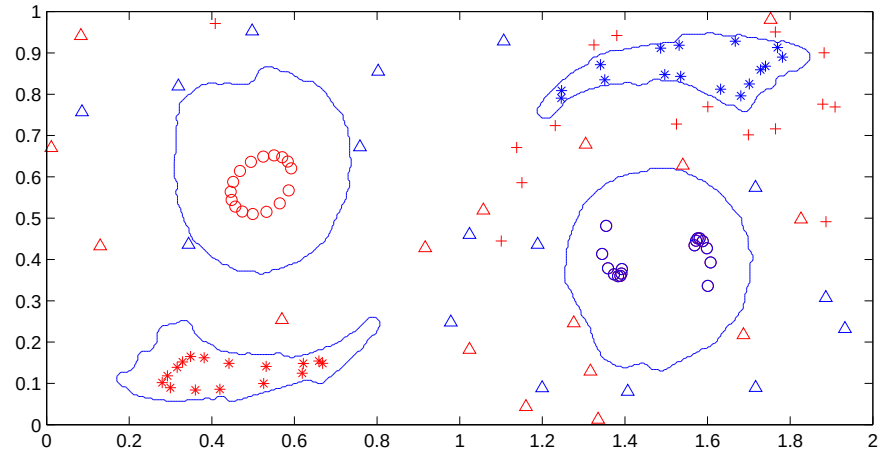

Figure 8: (Section 5.3 with $\epsilon=0.1$) Locations of particles at various times which are constant multiples of the period $T_m=10$. The boundaries of different partitions are plotted in blue.

Figure 9: (Section 5.3 with $\epsilon=0.1$) Ergodic partition of the double-gyre flow with $\epsilon=0.1$ at $t=2.5$.

integral F along trajectories will therefore be very different. This explains the dots in the background region in Figure 5. For those two triangular regions, FTLE are small and so the particle trajectories are insensitive to initial perturbations. Therefore the corresponding trajectory integral F have similar values.

5.4 Application to geometrical optics

Geometrical optics is an important class of asymptotic approximation to high frequency wave propagation. In the high frequency regime when $\omega\to\infty$, we approximate the phase function by the eikonal equation

$$|\nabla T|=\frac{1}{c}.$$

To obtain the multivalued solution to the traveltime field T in two dimensions, we reformulate the problem in the phase space by solving the eikonal equation using the Lagrangian formulation by the method of characteristics [7],

$$\begin{aligned}\frac{dx}{dt}&=c\sin\theta,\\ \frac{dy}{dt}&=c\cos\theta,\\ \frac{d\theta}{dt}&=c_y\sin\theta-c_x\cos\theta.\end{aligned}\tag{5.9}$$

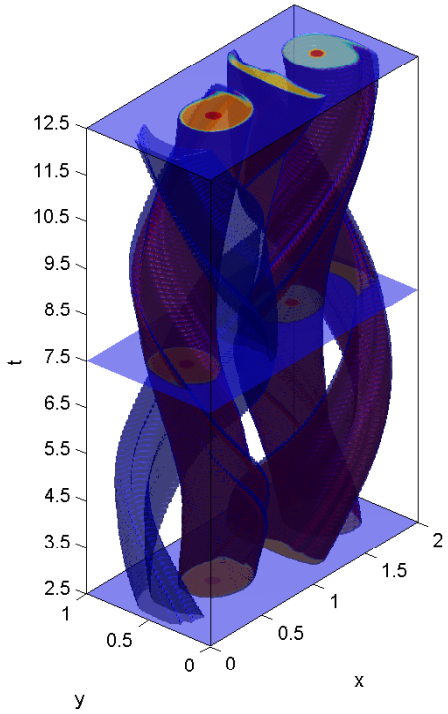

Figure 10: (Section 5.3 with $\epsilon=0.1$) The evolution of the clusters in Figure 9 from $t=2.5$ to $t=12.5$.

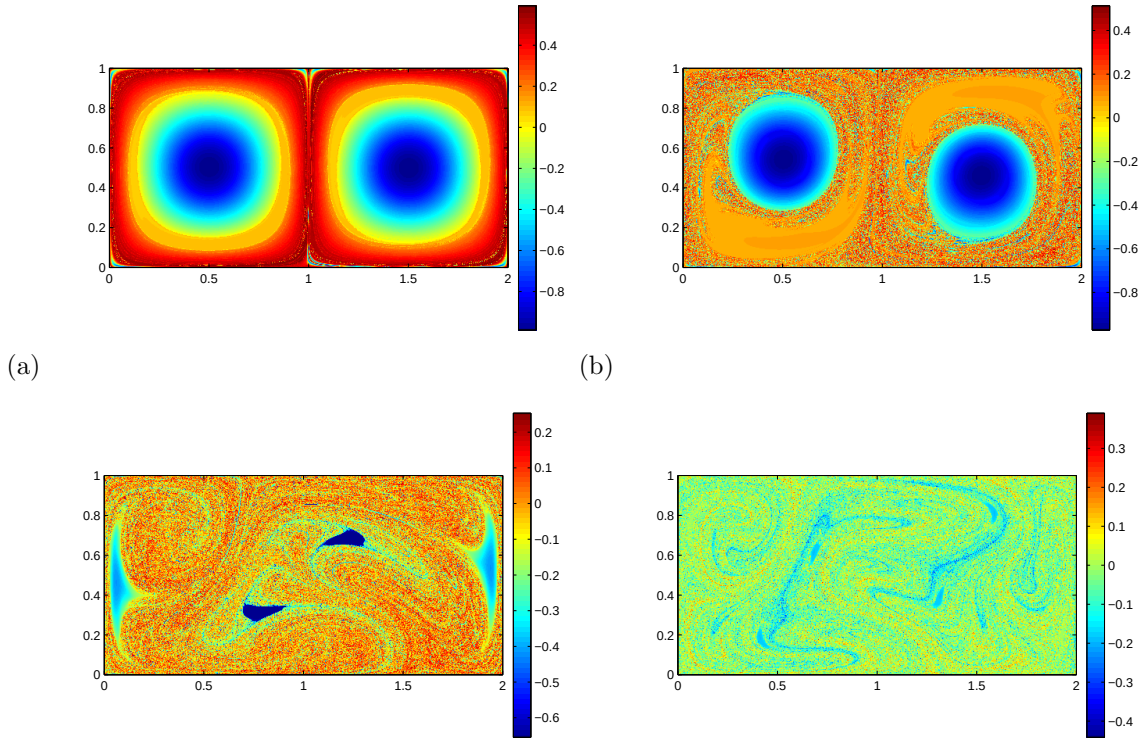

Figure 11: (Section 5.3) $\frac{1}{t_{ex}}F(\mathbf{x},t_{ex})$ with $f(\mathbf{x})=\cos(2\pi y)$ of the double-gyre flow with (a) $\epsilon=0.003$, (b) $\epsilon=0.05$, (c) $\epsilon=0.8$ and (d) $\epsilon=1.2$.

Unfortunately, this type of methods inherit the intrinsic shortcoming of other Lagrangian methods, rays emitting from even one single point (with different departure angles) could be very complex and compli-

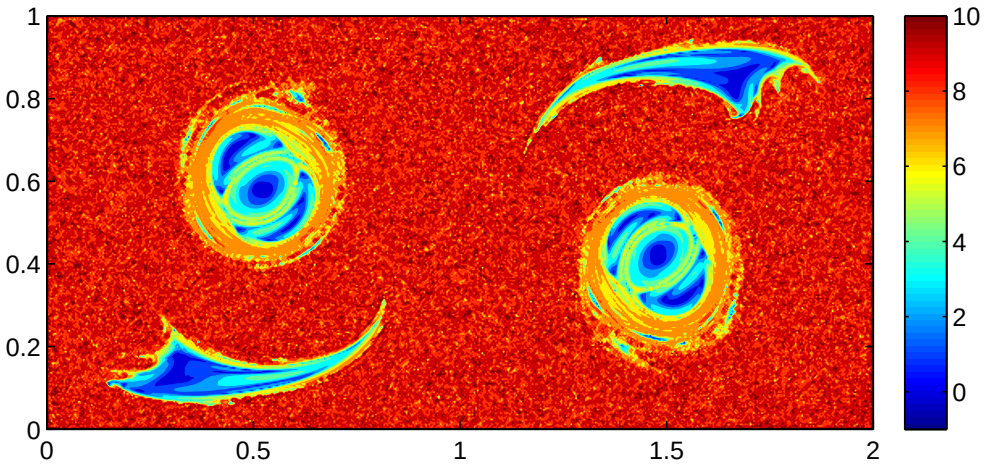

Figure 12: (Section 5.3 with $\epsilon=0.1$) Forward FTLE $\sigma^{320}(\mathbf{x},0)$.

cated, and hence, it is very unlikely that we can obtain a uniform resolution in the desired computational domain. One resolution of this is to dynamically add and remove rays (characteristics) as computation proceeds. Various adaptive ray tracing algorithms have been proposed to obtain a better resolved multivalued solution [40]. However, all these adaptive algorithms depend on certain quantity as a measure for inserting rays. For inhomogeneous velocity model, it is very usual to observe that the geometrical spreading increases exponentially in the distance from the source. It is therefore natural to consider the so-called Lyapunov exponent as a criteria for adaptivity [19].

In this section, we propose to use the coherent ergodic partition as another quantity to study the ray spreading by applying the ergodic partition theory and the corresponding algorithm we introduced above. We will try to couple these emitted rays into clusters. Characteristics classified into the same cluster should have very close behaviors. Therefore, theoretically in the adaptive method, one can simply refine the angle space near the boundaries of these clusters.

In many applications [10, 13, 35, 34], the traveltimes of interest are carried by the so-called sub-horizontal rays where one assumes rays are oriented in the positive y-direction. Therefore, we can use depth as the running parameter so that we have a reduced system

$$\begin{aligned}\frac{dx}{dy} &= \tan\theta,\\ \frac{d\theta}{dy} &= \frac{c_y}{c}\tan\theta-\frac{c_x}{c}.\end{aligned} \tag{5.10}$$

In this example, we consider $c=1+0.2\sin(0.5\pi y)\sin(3\pi(x+0.55))$ and so the flow is periodic in the y-direction with period $y_m=4$.

Since the velocity field is now y-dependent in the $x-\theta$ space, we first solve the above reduced ray tracing system up to $y=y_m$ and then compute the value of

$$F(x,\theta,y_m)\triangleq\int_0^{y_m} f\circ\phi_y(x,\theta)\,dy$$

to form our coherent ergodic clusters. In the left subfigure of Figure 13, we solve this reduced ray system up to $y=8$ with initial take-off angle ranging from -1 to 1. We can see clearly that rays already form clusters. On the right, we have shown the quantity $\frac{1}{8}F(x,\theta,8)$ and $f=\sin x$. If we focus on the cross section $x=0$ which corresponds to the rays emitting from the origin with different departure angles, we observe that there exists three subintervals $\theta\in[-0.4625,-0.18125]$, $[0.0625,0.125]$ and $[0.1375,0.21875]$ which share the same color. This suggests that rays emitting from one of these subintervals may travel as a patch in the y-direction, as demonstrated in Figure 14.

However, rays from other subintervals in the θ-direction may not form clusters. For instance, rays emitted from the origin with departure angles in $[-0.1,-0.05]$ or $[0.4,0.45]$ are very complex. As seen in Figure 15(a), the quantity $\frac{1}{y_m}F(0,\theta,y_m)$ changes rapidly inside these regions. If we consider rays with initial take-off angle inside these subintervals, we would expect these trajectories behave significantly different, as plotted in Figure 15(b) and (c). This demonstrates that the coherent ergodic partition

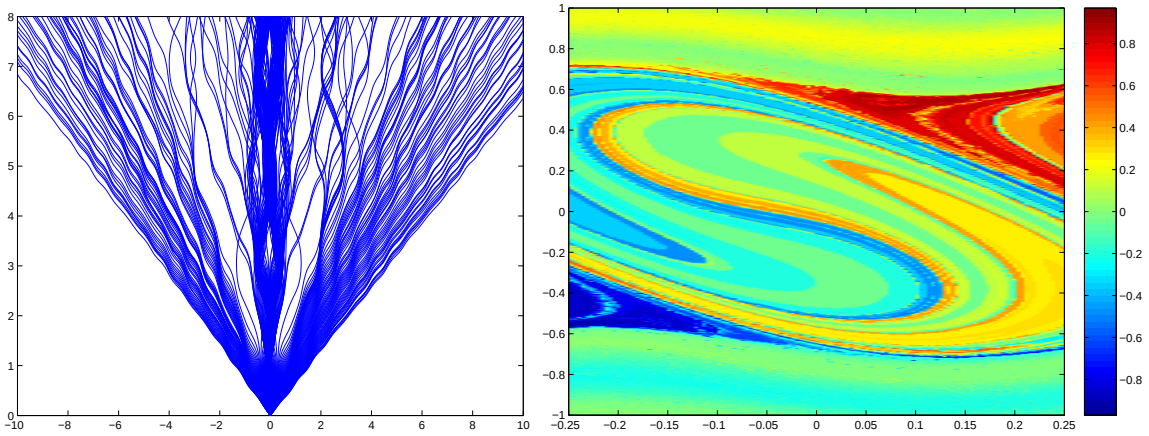

Figure 13: (Section 5.4) (Left) Rays emitting from the origin with different angles; (Right) The result of $\frac{1}{8}F(x,\theta,8)$ and $f=\sin x$.

provides a nice indicator for implementing an adaptive ray tracing. In particular, in the region where the quantity $\frac{1}{y_m}F(x_s,\theta,y_m)$ changes rapidly, we could locally insert more take-off rays from the point source $x=x_s$.

Another nice property of this Eulerian formulation is that we have already obtained the coherent ergodic partition for **all** rays shooting from **any** point source on the $y=0$ level. For example, to look at the partition from another source at $x=x_s$, one only needs to extract the previous solution $\frac{1}{y_m}F(x_s,\theta,y_m)$. For example, we consider the cross section of F along $x_s=-0.12$ which corresponds to rays emitted from the point $(x,y)=(-0.12,0)$ with different departure angles. Rays emitted from $(-0.12,0)$ with departure angle $\theta\in[-0.45,-0.4]\cup[0.05,0.1]$ are very complex. As seen in Figure 16(a), $\frac{1}{y_m}F(0,\theta,y_m)$ changes rapidly inside these regions. If we consider rays with initial take-off angle inside these subintervals, we would expect these trajectories behave significantly different, as plotted in Figure 16(b) and (c).

Acknowledgement

The work of Leung was supported in part by the Hong Kong RGC under Grants 602210 and 605612.

References

[1] V.I. Arnold and A. Avez. *Ergodic Problems of Classical Mechanics*. Addison-Wesley, 1968.

[2] M. Brin and S. Garrett. *Introduction to Dynamical Systems*. Cambridge University Press, 2002.

[3] M. Budisic and I. Mezic. Geometry of the ergodic quotient revels coherent structures in flows. *Physica D*, 241:1255–1269, 2012.

[4] E.J. Candès and L. Ying. Fast geodesics computation with the phase flow method. *J. Comput. Phys.*, 220:6–18, 2006.

[5] C. Carson, S. Belongie, H. Greenspan, and R. Malik. Blobworld: image segmentation using expectation-maximization and its application to image querying. *IEEE Trans. on Pattern Anal. Mach. Intell.*, 24(8):1026–1038, 2002.

[6] V. Caselles, R. Kimmel, and G. Sapiro. Geodesic active contours. *International Journal of Computer Vision*, 22(1):61–79, 1997.

[7] V. Cerveny, I. A. Molotkov, and I. Psencik. *Ray method in seismology*. Univerzita Karlova press, 1977.

[8] T. Chan and L. Vese. Active contours without edges. *IEEE Transactions on Image Processing*, 10:266–277, 2001.

[9] G.H. Choe. *Computational Ergodic Theory*. Springer-Verlag, 2005.

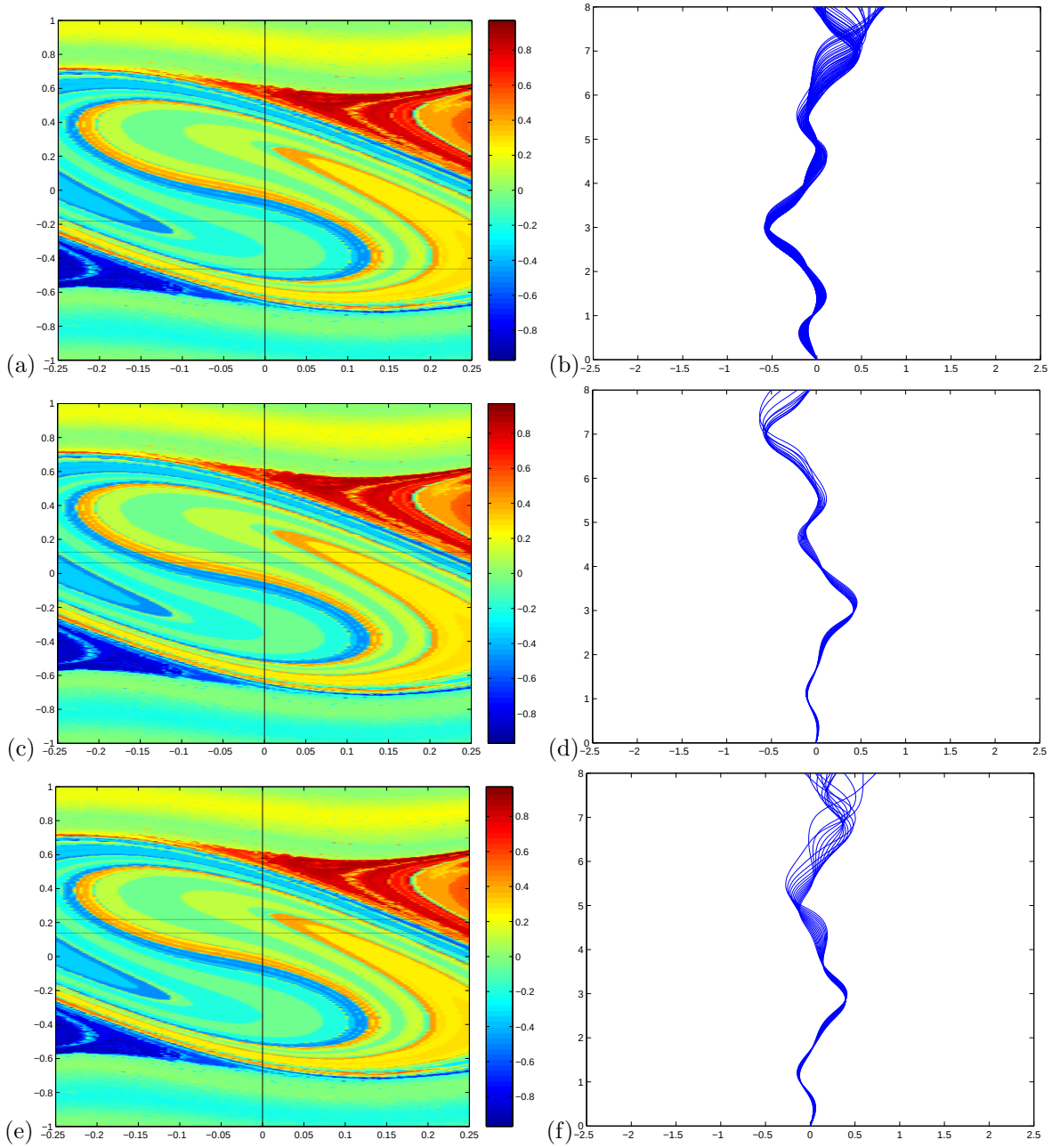

Figure 14: (Section 5.4) The angle subintervals sharing the same color are shown in (a)$[-0.4625, -0.18125]$, (c)$[0.0625, 0.125]$ and (e)$[0.1375, 0.21875]$; (b,d,f) clusters of rays emitted from the origin corresponding to (a), (c) and (e), respectively.

[10] J. F. Claerbout. *Fundamentals of geophysical data processing.* McGraw-Hill, 1976.

[11] G. Froyland and K. Padberg. Almost-invariant sets and invariant manifolds connecting probabilistic and geometric descriptions of coherent structures in flows. *Physica D*, 238(1507-1523), 2009.

[12] S. Gottlieb and C.-W. Shu. Total variation diminishing Runge-Kutta schemes. *Mathematics of Computation*, 67:73–85, 1998.

[13] S. Gray and W. May. Kirchhoff migration using eikonal equation traveltimes. *Geophysics*, 59:810–817, 1994.

[14] L. Gupta and T. Sortrakul. A gaussian-mixture-based image segmentation algorithm. *Pattern Recognition*, 31(3):315–325, 1998.

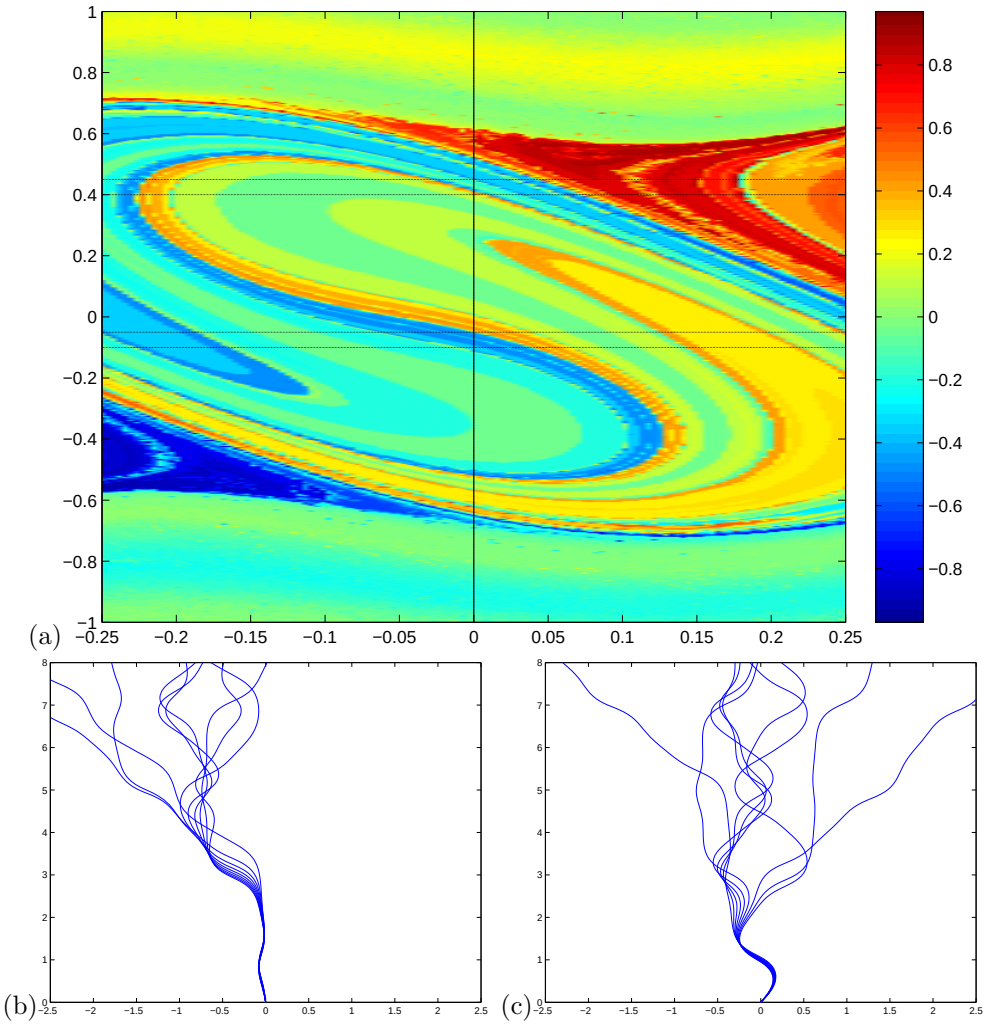

Figure 15: (Section 5.4) (a) $\frac{1}{y_m}F(0,\theta,y_m)$ varies significantly in the subintervals $\theta\in[-0.1,-0.05]$ and $[0.4,0.45]$. (b) Rays emitted from the origin with departure angles in $[-0.1,-0.05]$. (c) Rays emitted from the origin with departure angles in $[0.4,0.45]$.

[15] G. Haller. Distinguished material surfaces and coherent structures in three-dimensional fluid flows. *Physica D*, 149:248–277, 2001.

[16] G. Haller. Lagrangian structures and the rate of strain in a partition of two-dimensional turbulence. *Phys. Fluids A*, 13:3368–3385, 2001.

[17] G. Haller and T. Sapsis. Lagrangian coherent structures and the smallest finite-time Lyapunov exponent. *Chaos*, 21, 2011.

[18] G. Haller and G. Yuan. Lagrangian coherent structures and mixing in two-dimensional turbalence. *Physica D*, 147:352–370, 2000.

[19] L. Klimes. Lyapunov exponents for 2-d ray tracing without interfaces. *Pure appl.geophys.*, 159:1465–1485, 2002.

[20] J.L. Lebowitz and O. Penrose. Modern ergodic theory. *Physics Today*, 26:23–29, 1973.

[21] S. Leung. Eulerian approach for computing the finite time Lyapunov exponent. *J. Comput. Phys.*, 230:3500–3524, 2011.

[22] S Leung. A backward phase flow method for the finite time lyapunov exponent. *Submitted*, 2012.

[23] S. Leung, G. Liang, K. Solna, and H.K. Zhao. Expectation-maximization algorithm with local adaptivity. *SIAM Journal on Imaging Sciences*, 2:834–857, 2008.

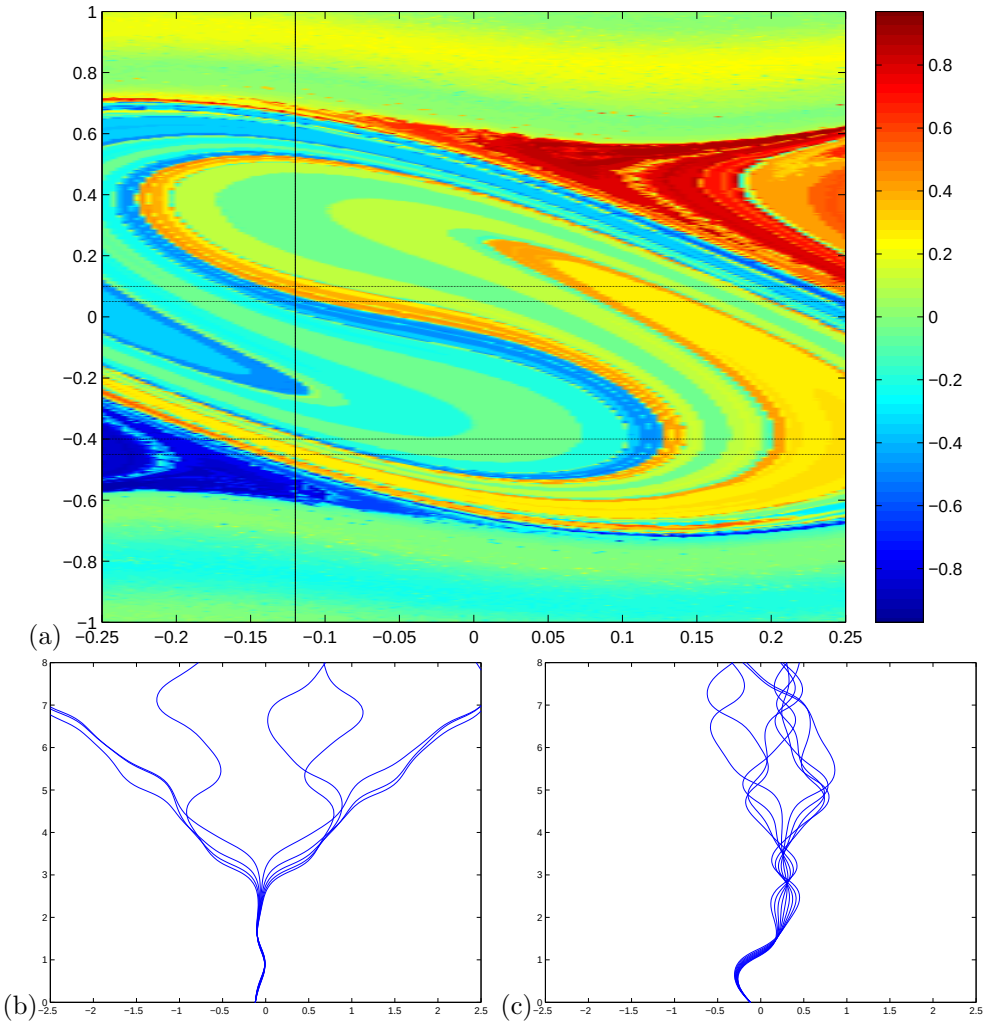

Figure 16: (Section 5.4) (a) $\frac{1}{y_m}F(-0.12,\theta,y_m)$ varies significantly in the subintervals $\theta\in[-0.45,-0.4]$ and $[0.05,0.1]$. (b) Rays emitted from $(-0.12,0)$ with departure angles in $[-0.45,-0.4]$. (c) Rays emitted from the origin with departure angles in $[0.05,0.1]$.

[24] S. Leung and J. Qian. The backward phase flow and FBI-transform-based Eulerian Gaussian beams for the Schrödinger equation. *J. Comput. Phys.*, 229:8888–8917, 2010.

[25] Z. Levnajic and I. Mezic. Ergodic theory and visualization i: Mesochronic plots for visualization of ergodic partition and invariant sets. *Chaos*, 20:033114, 2010.

[26] Z. Levnajic and I. Mezic. Ergodic theory and visualization ii:visualization of resonances and periodic sets. *e-print arXiv:1206.3164*, 2013.

[27] J. Liu, Y.B. Ku, and S. Leung. Expectation-maximization algorithm with total variation regularization for vector-valued image segmentation. *Journal of Visual Communication and Image Representation*, pages 1234–1244, 2012.

[28] X. D. Liu, S. J. Osher, and T. Chan. Weighted Essentially NonOscillatory schemes. *J. Comput. Phys.*, 115:200–212, 1994.

[29] I. Mezic. On the geometrical and statistical properties of dynamical systems : theory and applications. *Caltech Ph.D. Thesis*, 1994.

[30] I. Mezic and S. Wiggins. A method for visualization of invariant sets of dynamical systems based on the ergodic partition. *Chaos*, 9:213–218, 1999.

[31] P.K. Newton. *The N-Vortex Problem: Analytical Techniques*. Springer-Verlag, 2001.

[32] S. J. Osher and J. A. Sethian. Fronts propagating with curvature dependent speed: algorithms based on Hamilton-Jacobi formulations. *J. Comput. Phys.*, 79:12–49, 1988.

[33] H. Permuter, J. Francos, and I. Jermyn. A study of gaussian mixture models of color and texture features for image classification and segmentation. *Pattern Recognition*, 39(4):695–706, 2006.

[34] J. Qian and S. Leung. A level set based Eulerian method for paraxial multivalued traveltimes. *J. Comput. Phys.*, 197:711–736, 2004.

[35] J. Qian and W. W. Symes. Adaptive finite difference method for traveltime and amplitude. *Geophysics*, 67:167–176, 2002.

[36] L. Rudin, S.J. Osher, and E. Fatemi. Nonlinear total variation based noise removal algorithms. *Physica D*, 60:259–268, 1992.

[37] S.C. Shadden, F. Lekien, and J.E. Marsden. Definition and properties of Lagrangian coherent structures from finite-time Lyapunov exponents in two-dimensional aperiodic flows. *Physica D*, 212:271–304, 2005.

[38] C. W. Shu. Essentially non-oscillatory and weighted essentially non-oscillatory schemes for hyperbolic conservation laws. In B. Cockburn, C. Johnson, C.W. Shu, and E. Tadmor, editors, *Advanced Numerical Approximation of Nonlinear Hyperbolic Equations*, volume 1697, pages 325–432. Springer, 1998. Lecture Notes in Mathematics.

[39] Y. Susuki and I. Mezic. Ergodic partition of phase space in continuous dynamical systems. *IEEE Conference on Decision and Control and 28th Chinese Control Conference*, pages 7497–7502, 2009.

[40] V. Vinje, E. Iversen, and H. Gjoystdal. Traveltime and amplitude estimation using wavefront construction. *Geophysics*, 58:1157–1166, 1993.

[41] P. Walters. *An Introduction to Ergodic Theory.* Springer-Verlag, 1982.